







Rydberg-atom experiment for the integer factorization problem

Juyoung Park ¹, Seokho Jeong ¹, Minhyuk Kim ^{1,2}, Kangheun Kim ¹, Andrew Byun,¹ Louis Vignoli ³,
Louis-Paul Henry,³ Loïc Henriët,³ and Jaewook Ahn ¹

¹Department of Physics, KAIST, Daejeon 34141, Republic of Korea

²Department of Physics, Korea University, Seoul 02841, Republic of Korea

³PASQAL, 7 rue Léonard de Vinci, 91300 Massy, France



(Received 5 February 2024; accepted 16 May 2024; published 4 June 2024)

The task of factoring integers poses a significant challenge in modern cryptography, and quantum computing holds the potential to efficiently address this problem compared to classical algorithms. Thus, it is crucial to develop quantum computing algorithms to address this problem. This study introduces a quantum approach that utilizes Rydberg atoms to tackle the factorization problem. Experimental demonstrations are conducted for the factorization of small composite numbers such as $6 = 2 \times 3$, $15 = 3 \times 5$, and $35 = 5 \times 7$. This approach involves employing Rydberg-atom graphs to algorithmically program binary multiplication tables, yielding many-body ground states that represent superpositions of factoring solutions. Subsequently, these states are probed using quantum adiabatic computing. Limitations of this method are discussed, specifically addressing the scalability of current Rydberg quantum computing for the intricate computational problem.

DOI: [10.1103/PhysRevResearch.6.023241](https://doi.org/10.1103/PhysRevResearch.6.023241)

I. INTRODUCTION

Modern cryptosystems using public-key distribution rely on the fact that finding prime factors, p and q , of a given semiprime integer, $n = p \times q$, is computationally inefficient in classical computation [1]. On a quantum computer, Shor's algorithm is expected to run in a polylogarithmic time of n , i.e., to solve the factorization problem efficiently [2,3]. Experimental tests of Shor's algorithm for small integers have been conducted on various quantum gate-based computers, including those using NMR [4], trapped ions [5], superconductor qubits [6,7], and photons [8,9]. Improvements are expected in gate fidelity and system size to facilitate factorization of larger numbers. An alternative approach is provided by quantum adiabatic computing [10], where the integer factorization problem is encoded into the Hamiltonian of a quantum many-body system, which allows the prime factors to be obtained by adiabatically driving the system to its ground state. Experimentally quantum adiabatic methods are carried out with NMR systems [11,12] as well as on commercially accessible platforms such as IBMQ [13] and D-Wave [14]. These experiments utilize quadratic unconstrained binary optimization (QUBO) to encode the factorization problem into Hamiltonians.

In recent years, there has been a rapid progress in the field of Rydberg-atom-based quantum computing [15–18]. Atomic qubits numbering in the hundreds have become available and are used for various quantum applications, including quantum simulations, adiabatic quantum computing, and quantum approximate optimization algorithms [19–25]. The

versatility of atom rearrangement techniques has enabled the creation of highly customizable atomic arrangements in conjunction with either quantum wires [26,27], crossing gadgets [28,29] utilizing local addressing [25,30,31], or a dynamic qubit architecture [22,24]. Experimentally, Rydberg-atom graphs, each denoted as $G(V, E)$, where V represents atoms and E denotes pairwise strong Rydberg couplings, are applied to nondeterministic polynomial time (NP)-complete problems including the maximum independent set (MIS), maximum cut, and satisfiability (SAT) problems [25,26,32–34].

This paper aims to program Rydberg-atom graphs for solving the integer factorization problem and experimentally determining its factors. Of particular relevance in the context of this paper, previous theoretical considerations have explored the use of Rydberg-atom systems employing crossing gadgets and single-atom addressing [28]. In this work, we opt for constructing Rydberg-atom graphs using three-dimensional structures and quantum wires instead of relying on the technically challenging single addressing.

The procedure involves an efficient two-step reduction algorithm that transforms the integer factorization problem, via (i) the SAT problem, into (ii) the MIS problem. Additionally, it includes a protocol for embedding the MIS problem onto a Rydberg-atom graph and experimentally probing the Rydberg-atom graph's ground state. The subsequent sections of the paper elaborate on the procedure, starting with an overview of the use of a Rydberg-atom graph in integer factorization, illustrated by the example of $p \times q = 6$ in Sec. II. Details about encoding of the factorization into the SAT problem are provided in Sec. III. Experimental demonstrations of $p \times q = 15$ and 35 are presented in Sec. IV. Scalability issues related to the Rydberg-atom approach to the integer factorization problem are discussed in Sec. V, leading to conclusions in Sec. VI.

Published by the American Physical Society under the terms of the [Creative Commons Attribution 4.0 International](https://creativecommons.org/licenses/by/4.0/) license. Further distribution of this work must maintain attribution to the author(s) and the published article's title, journal citation, and DOI.

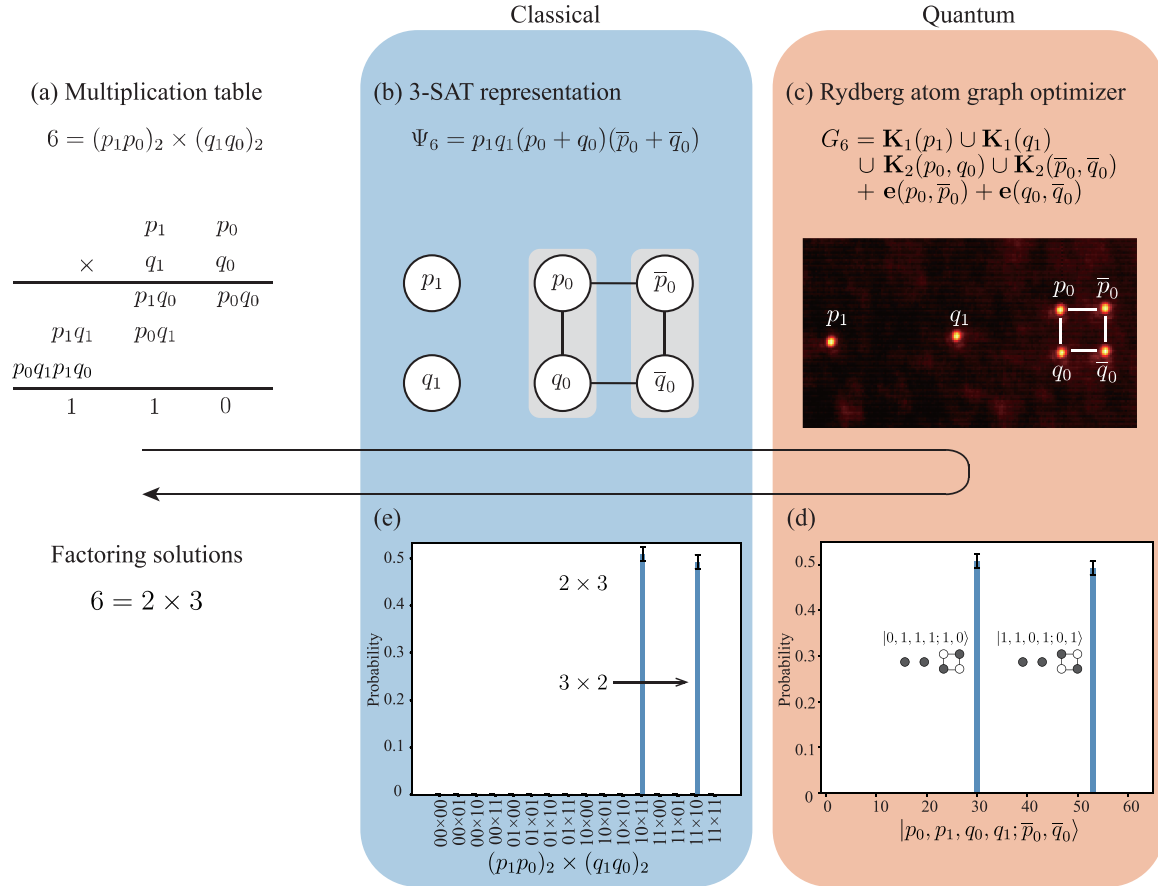


FIG. 1. The procedure of addressing the integer factorization problem using a Rydberg-atom graph. (a) The instance $p \times q = 6$ and its associated multiplication table. (b) The 3-satisfiability (3-SAT) representation of the given factoring problem, along with the corresponding graph G_6 . (c) Implementation of Rydberg-atom quantum adiabatic computing, where G_6 is manifested as a Rydberg-atom graph. (d),(e) Experimental probability distributions in $|p_0, p_1, q_0, q_1; \bar{p}_0, \bar{q}_0\rangle$ basis and $(p_1p_0)_2 \times (q_1q_0)_2$ basis, respectively.

II. RYDBERG-ATOM APPROACH TO THE INTEGER FACTORIZATION PROBLEM

We describe the method of programming the integer factorization problem with a Rydberg-atom graph, using the simplest possible example of $p \times q = 6$ as illustrated in Fig. 1. Initially, we reduce the integer factorization problem to a SAT one. Considering the three-bit binary representation $6 = (110)_2$, we assume that the factors p and q are two-bit integers, denoted as $p = (p_1p_0)_2$ and $q = (q_1q_0)_2$. The Boolean equations governing the binary variables p_0, p_1, q_0, q_1 are then derived from the multiplication table in Fig. 1(a) as follows:

$$p_0q_0 = 0, \quad (1a)$$

$$p_0q_1 \oplus p_1q_0 = 1, \quad (1b)$$

$$p_0q_1p_1q_0 \oplus p_1q_1 = 1, \quad (1c)$$

where \oplus is XOR and $p_0q_1p_1q_0$ in Eq. (1c) denotes the carry arising from Eq. (1b). These equations can be efficiently (i.e., in a polynomial number of steps in the bit number of n) converted to a Boolean equation in conjunctive normal form,

yielding

$$\Psi_6 = p_1q_1(p_0 + q_0)(\bar{p}_0 + \bar{q}_0) = 1. \quad (2)$$

Further details will be described in Sec. III. The Boolean equation $\Psi_6 = 1$ readily translates into the following Boolean satisfiability (SAT) problem of four clauses:

$$\Psi_6(p_0, p_1, q_0, q_1) = C_1 \wedge C_2 \wedge C_3 \wedge C_4 = 1, \quad (3a)$$

$$C_1 = p_1, \quad (3b)$$

$$C_2 = q_1, \quad (3c)$$

$$C_3 = p_0 \vee q_0, \quad (3d)$$

$$C_4 = \bar{p}_0 \vee \bar{q}_0. \quad (3e)$$

Subsequently, we translate this SAT problem into a MIS problem on a graph, as depicted in Fig. 1(c). The first two clauses C_1 and C_2 in Eqs. (3b) and (3c) are incorporated into isolated single-vertex graphs denoted as \mathbf{K}'_1 s in graph nomenclature:

$$\mathbf{K}_1(v) := G(V = \{v\}, E = \emptyset). \quad (4)$$

For C_3 and C_4 , two-vertex connected graphs, or \mathbf{K}'_2 s, are employed:

$$\mathbf{K}_2(v_1, v_2) := G(V = \{v_1, v_2\}, E = \{(v_1, v_2)\}). \quad (5)$$

Now, we introduce additional edges to represent interclause relations between variables p_0, q_0 and their negations \bar{p}_0, \bar{q}_0 , creating connections between C_3 and C_4 . These interclause edges impose constraints between the vertices encoding the same variables. Consequently, the graph G_6 expressing the factorization problem $p \times q = 6$ as a MIS problem on the graph is defined as follows:

$$G_6 = \mathbf{K}_1(p_1) \cup \mathbf{K}_1(q_1) \cup \mathbf{K}_2(p_0, q_0) \cup \mathbf{K}_2(\bar{p}_0, \bar{q}_0) + \mathbf{e}(p_0, \bar{p}_0) + \mathbf{e}(q_0, \bar{q}_0). \quad (6)$$

Here, G_6 has maximum independent set of size 4, which is equal to the number of clauses in Ψ_6 . Therefore, any maximum independent set configuration of size 4 corresponds to an assignment satisfying $\Psi_6 = 1$, ensuring that the corresponding binary representation of numbers p, q meet $p \times q = 6$.

By transforming the integer factorization problem into a MIS one, we can leverage a Rydberg-atom experiment to address it, exploiting the Rydberg blockade phenomenon to inherently encode the independence condition in the spatial configuration of the atoms. Specifically, the graph G_6 is implemented as a Rydberg-atom graph, where each vertex corresponds to an atom, and edges are established by positioning the respective pairs of atoms in close proximity, ensuring that their simultaneous excitation to the Rydberg state is hindered by the blockade phenomenon [35,36]. Following a quantum evolution, the collection of atoms in the Rydberg state delineates a subset of vertices of G_6 . These subsets sampled from this final state are expected to be good candidates for the MIS of the graph.

The Hamiltonian is defined for a general graph G (an unweighted graph) as follows:

$$\hat{H}(G) = \frac{U}{4} \sum_{(j,k) \in E} (\hat{\sigma}_z^{(j)} + 1)(\hat{\sigma}_z^{(k)} + 1) - \frac{\hbar\Delta}{2} \sum_{j \in V} \hat{\sigma}_z^{(j)}, \quad (7)$$

where $|0\rangle$ and $|1\rangle$ are pseudospin states denoting the ground and Rydberg-atom states, respectively, $\hat{\sigma}_z = |1\rangle\langle 1| - |0\rangle\langle 0|$, U is the interaction between each pair of “edged” atoms (of the same separation distance), and Δ is the detuning of Rydberg-atom excitation. The MIS phase requires two conditions: $U \gg \hbar|\Delta|$ enforces the Rydberg blockade phenomenon; and $\Delta > 0$ maximizes the number of atoms being excited to the Rydberg state. The many-body ground state $|\hat{H}(G)\rangle$ is then the superposition of MIS’s of G [26,37]. For the Rydberg-atom graph G_6 in Eq. (6), the many-body ground state $|\hat{H}(G_6)\rangle$ of $\hat{H}(G_6)$ is given by

$$|\hat{H}(G_6)(|p_0 p_1 q_0 q_1; \bar{p}_0 \bar{q}_0)\rangle = \frac{|0111; 10\rangle + |1101; 01\rangle}{\sqrt{2}}, \quad (8)$$

which is the superposition of two factoring solutions, $p \times q = (10)_2 \times (11)_2$ and $(11)_2 \times (10)_2$.

Experimental verification can be performed with the adiabatic evolution of the Rydberg-atom graph G_6 from the paramagnetic phase to the antiferromagnetic phase, which corresponds to the MIS phase [33]. (See experimental details in Appendix A). We used rubidium atoms (^{87}Rb) with ground state $|0\rangle \equiv |5S_{1/2}, F=2, m_F=2\rangle$ and Rydberg state $|1\rangle \equiv |71S_{1/2}, m_J=1/2\rangle$. The Rabi frequency Ω is ramped up from 0 to $\Omega_0 = (2\pi)1.5$ MHz, while the laser detuning is maintained at $\Delta = -(2\pi)3.5$ MHz for 0.3 μs . Then the detuning is

ramped up from $-(2\pi)3.5$ to $+(2\pi)\delta_F$ MHz for 2.4 μs , with $\delta_F = 3.5$ and fixed Rabi frequency Ω_0 . (The $p \times q = 15$ and 35 experiments in Sec. IV are performed with $\delta_F = 3.5$ and 3.9, respectively.) Finally the Rabi frequency is ramped down to zero and the detuning is maintained at $+(2\pi)3.5$ MHz for 0.3 μs . The entire evolution time is 3.0 μs . The detuning and Rabi frequencies are changed with the frequency and the power of the excitation lasers with acousto-optic modulators (AOM), which are controlled by a programmable radio-frequency synthesizer (Moglabs XRF). After the quasia-adiabatic evolution, the population of each atom is measured by illuminating the conventional cycling transition lights where the atoms in the ground state show fluorescence whereas the atoms in the Rydberg state do not. The experimental results obtained with G_6 are depicted in Fig. 1(d), where the expected states $|p_0 p_1 q_0 q_1; \bar{p}_0 \bar{q}_0\rangle = |0111; 10\rangle$ and $|1101; 01\rangle$ in Eq. (8) are measured with high probabilities, confirming that the integer factors are $(11)_2 = 3$ and $(10)_2 = 2$.

III. ENCODING INTEGER FACTORIZATION INTO THE SATISFIABILITY PROBLEM

The conjunctive normal form of integer multiplication can be efficiently represented using a binary decision diagram (BDD), as detailed in Ref. [38]. In this context, we provide a concise overview of the BDD construction process, utilizing the example of $p \times q = 6$ in Sec. II, and derive Ψ_6 in Eq. (3), the Boolean expression in conjunctive normal form for the SAT problem [39,40].

In a generic factorization problem for a given semiprime number $n = p \times q$, if n is an N -bit integer, finding the unknown factors, p (an N_p -bit integer) and q (an N_q -bit integer), involves identifying the preimage of n through the binary multiplication function

$$f : \{0, 1\}^{N_p} \times \{0, 1\}^{N_q} \rightarrow \{0, 1\}^N, \quad (9)$$

where $N_q \geq N - N_p$. Let p_i ($0 \leq i \leq N_p - 1$) be the i th bit of p , q_j ($0 \leq j \leq N_q - 1$) the j th bit of q , and n_k ($0 \leq k \leq N - 1$) the k th bit of n . The function f is then expressed as

$$n = f(p_0, p_1, \dots, q_0, q_1, \dots) = \sum_{i=0}^{N_p-1} \sum_{j=0}^{N_q-1} p_i q_j 2^{i+j}, \quad (10)$$

where each term $p_i q_j 2^{i+j}$ contributes a nonzero value to the sum only when $p_i = q_j = 1$.

Figure 2(a) shows the BDD for the $p \times q = 6$ factoring problem. In this constructed BDD, each column corresponds to one of the three bit-wise calculations of $p \times q = 6$ in Eq. (1). There are three columns comprising a total of 10 unit BDDs, interconnected based on the constraints from bit-wise equations in Eq. (10). Assuming that we have processed the sum in Eq. (10) up to the (i, j) th term, by defining a running sum $f_{(i,j)} = v$, the subsequent running sum $f_{(i',j')}$ is given by

$$f_{(i',j')}(p_{i'}, q_{j'}; v) = \begin{cases} v & \text{if } p_{i'} q_{j'} = 0, \\ v + 2^{i'+j'} & \text{if } p_{i'} = q_{j'} = 1. \end{cases} \quad (11)$$

These running sum relations can be represented by the unit BDD, as depicted in Fig. 2(b). The starting and ending nodes contains the running values $f_{(i,j)}$ and $f_{(i',j')}$, respectively, with edges distinguished as solid or dotted based on whether the

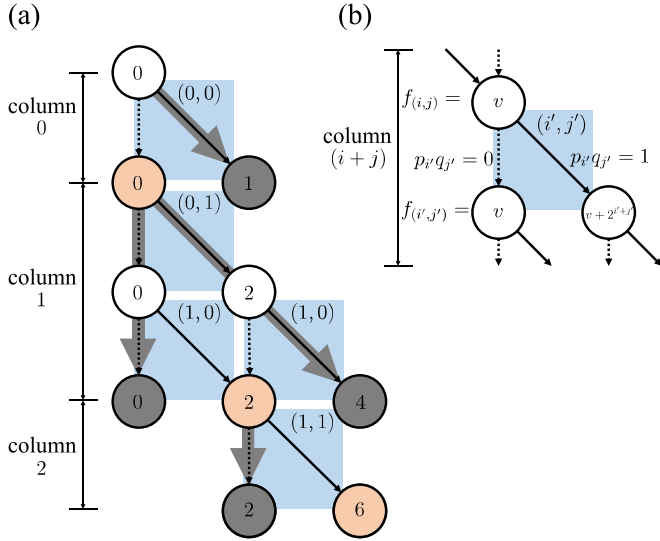


FIG. 2. (a) The binary decision diagram (BDD) for factoring $p \times q = 6$. (b) The unit BDD representing the logical relation between p_i and q_j in the multiplication table, depicted by the blue-colored box labeled $f_{(i',j')}$, where the edges in the BDD can be either solid or dotted, depending on whether $p_i q_j$ is 1 or 0.

product $p_i q_j$ is set to 1 or 0, respectively. The BDD for f is formed by linking these unit BDDs representing all running sum relations.

The first column (column 0) in Fig. 2(a) pertains to the first bit calculation, utilizing the topmost unit BDD to compute the running sum $f_{(0,0)}(p_0, q_0) = p_0 q_0$. Two possible end node values, $f_{(0,0)} = 0$ (derived from paths satisfying $p_0 q_0 = 0$) and $f_{(0,0)} = 1$ (through the path of $p_0 q_0 = 1$), emerge. Only the former (the orange-colored, left end node) aligns with the first bit constraint $f_{(0,0)} = n_0$, leading to the exclusion of the latter (the gray-colored, right end node). The second column (column 1) initiates from the $f_{(0,0)} = 0$ node and computes the second bit of n . Three possible end nodes represent the running sums $f_{(1,0)} = 0, 2$, and 4 , respectively. Among these, only the second one satisfies the second bit equation $f_{(1,0)} = n_0 + n_1 \times 2$. Similarly, the third column (column 2) begins from the $f_{(1,0)} = 2$ node and terminates at two possible nodes, $f_{(1,1)} = 2$ and 6 . The second one is the only one satisfying $f_{(1,1)} = n_0 + n_1 \times 2 + n_2 \times 2^2$.

Now we seek a Boolean expression in conjunctive normal form for the 3-SAT problem. Generally, the prime number couple (p, q) for a semiprime number $n = p \times q$ is unique (up to ordering). So, the determination of BDD paths leading to the end node corresponding to n establishes the values of p_i s and q_j s. Since p_i s and q_j s are involved in various paths, fixing their values imposes constraints on the BDD paths. Conversely, preventing certain paths from extending beyond the solution space by incorrectly setting a bit-wise equation for n_i introduces constraints on the potential values of p_i s and q_j s. Aggregating these constraints enables the representation of the given factorization problem through a Boolean formula of the SAT problem.

In the illustrated BDD example in Fig. 2(a), the paths (gray arrows) unable to meet the constraints are as follows: $p_0 q_0 = 1$ in column 0, $\overline{p_0 q_1} \cdot \overline{p_1 q_0} = 1$ and $p_0 q_1 p_1 q_0 = 1$ in

column 1, and $q_2 = 1$, $\overline{p_1 q_1} = 1$, and $p_2 = 1$ in column 2. These unsuccessful paths, which are the gray-colored arrows in Fig. 2(b), can be expressed in disjunctive norm form as follows:

$$\neg \Psi_{6,0} = p_0 q_0, \quad (12a)$$

$$\neg \Psi_{6,1} = \overline{p_0 q_1} \cdot \overline{p_1 q_0} + p_0 q_1 p_1 q_0, \quad (12b)$$

$$\neg \Psi_{6,2} = \overline{p_1 q_1}. \quad (12c)$$

The resulting Boolean equation for $p \times q = 6$ is given by

$$\begin{aligned} \Psi_6 &= \neg(\neg \Psi_{6,0} + \neg \Psi_{6,1} + \neg \Psi_{6,2}) \\ &= p_1 q_1 (p_0 + q_0) (\overline{p_0} + \overline{q_0}) = 1, \end{aligned} \quad (13)$$

which is the same as Ψ_6 in Eq. (2) in Sec. II.

IV. EXPERIMENTAL DEMONSTRATION

We now apply the process of translating factoring problems into Rydberg-atom graphs to experimentally investigate the integer factors of $p \times q = 15$ and $p \times q = 35$. We first derive the corresponding Boolean expressions in conjunctive normal form using the methodology outlined in Sec. III and subsequently these expressions are transformed into their respective Rydberg-atom graphs.

A. Solving $p \times q = 15$

The conjunctive normal form Boolean equation representing $p \times q = 15$ is derived as follows:

$$\begin{aligned} \Psi_{15} &= (p_1 + p_2)(q_1 + q_2)(p_1 + q_1)(\overline{p_1} + \overline{q_1}) \\ &\quad \times (p_1 + \overline{p_2} + \overline{q_2})(q_1 + \overline{p_2} + \overline{q_2}) p_0 q_0 = 1. \end{aligned} \quad (14)$$

The detailed construction of Ψ_{15} from the BDD is described in Appendix C. The corresponding Rydberg-atom graph G_{15} is then expressed as

$$\begin{aligned} G_{15} &= \mathbf{K}_2(p_1^{(1)}, p_2) \cup \mathbf{K}_2(q_1^{(1)}, q_2) \cup \mathbf{K}_2(p_1^{(2)}, q_1^{(2)}) \\ &\quad \cup \mathbf{K}_2(\overline{p_1}, \overline{q_1}) \cup \mathbf{K}_3(p_1^{(3)}, \overline{p_2}^{(1)}, \overline{q_2}^{(1)}) \\ &\quad \cup \mathbf{K}_3(q_1^{(3)}, \overline{p_2}^{(2)}, \overline{q_2}^{(2)}) \\ &\quad + \sum_{i=1,2,3} \mathbf{e}(p_1^{(i)}, \overline{p_1}) + \sum_{j=1,2} \mathbf{e}(p_2, \overline{p_2}^{(j)}) \\ &\quad + \sum_{i=1,2,3} \mathbf{e}(q_1^{(i)}, \overline{q_1}) + \sum_{j=1,2} \mathbf{e}(q_2, \overline{q_2}^{(j)}), \end{aligned} \quad (15)$$

which is depicted in Fig. 3(a). Each parenthesized term in Ψ_{15} corresponds to a two- or three-vertex connected graph (\mathbf{K}_2 or \mathbf{K}_3), and each variable-negation relation is represented by an additional edge. The superscript indices in the last four terms in Eq. (15) denote variable-atom duplicates in different subgraphs (\mathbf{K}_2 or \mathbf{K}_3). The single-vertex graphs for p_0 and q_0 are omitted in Fig. 3(a), for simplicity.

The graph G_{15} is not directly implementable with a two-dimensional (2D) arrangement of atoms. To address this, we opt for a three-dimensional (3D) atomic arrangement, following the approach outlined in Refs. [41,42]. The resulting experimental Rydberg-atom graph G_{15}^{EXP} is illustrated in Fig. 3(b). The graph features a three-layer atomic structure: the top layer contains three variables $p_1^{(1)}, p_1^{(2)}, q_1^{(2)}$; the

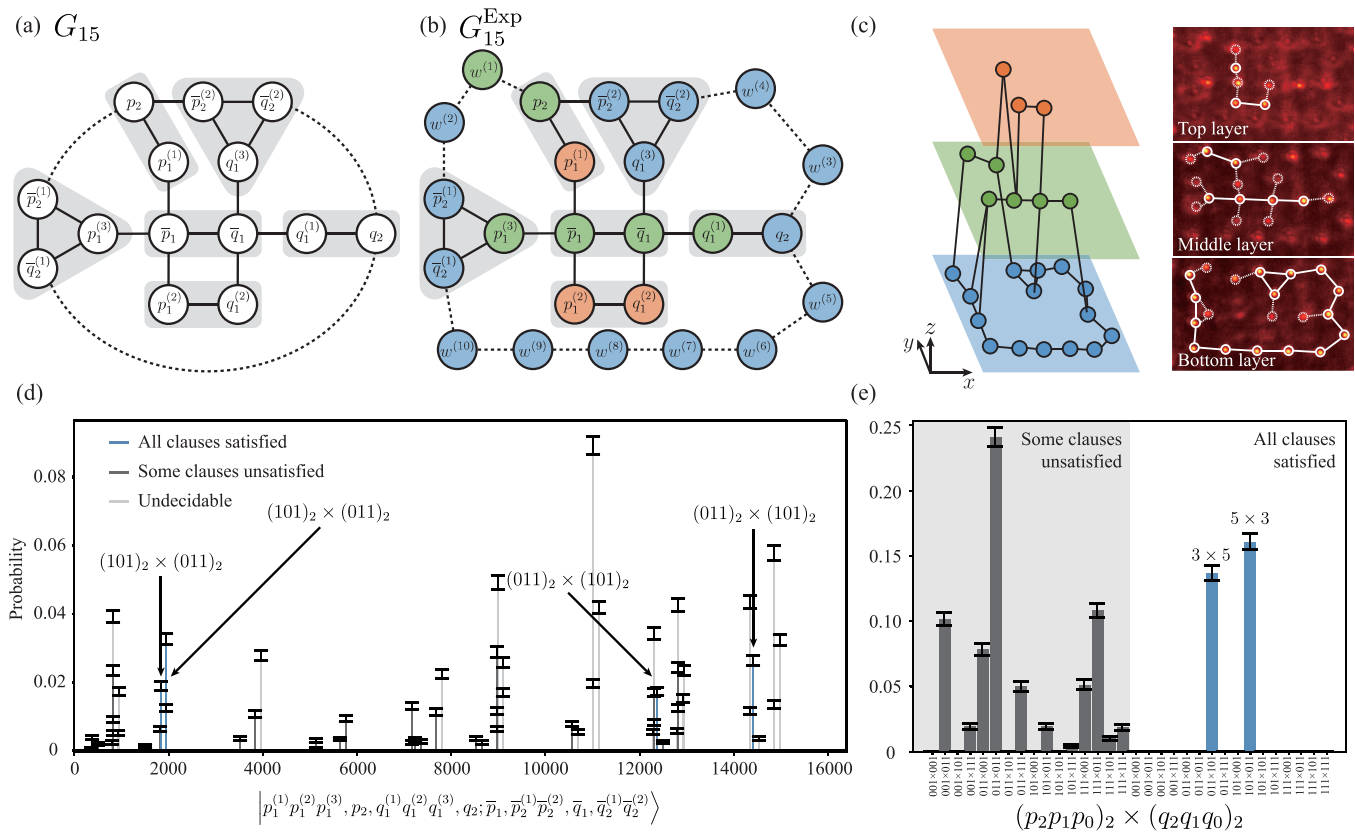


FIG. 3. Implementing the integer factorization of $p \times q = 15$ using Rydberg atoms. (a) Rydberg-atom graph G_{15} . (b) Experimental Rydberg-atom graph G_{15}^{Exp} and (c) image of atoms in 3D configuration. (d) Experimental probability distribution for all microstates in the basis of variable and negation atoms of G_{15}^{Exp} . The four blue peaks are $|000, 1, 111, 0\rangle; |100010\rangle$ corresponding to $((p_2 p_1 p_0)_2, (q_2 q_1 q_0)_2) = (101; 011), |111, 0, 000, 1\rangle; |0, 01, 1, 00\rangle$ corresponding to $(011; 101), |000, 1, 110, 0\rangle; |1, 00, 0, 11\rangle$ corresponding to $(101; 011)$, and $|110, 0, 000, 1\rangle; |0, 11, 1, 00\rangle$ corresponding to $(011; 101)$. (e) Result of factorization. The portion of peaks in (d) following the 3-SAT logical constraints is mapped to $(011; 101) = (3, 5)$ and $(101, 011) = (5, 3)$, demonstrating the correct answer to the factoring problem $15 = 3 \times 5$.

middle layer encompasses five variables $p_2, \bar{p}_1, p_1^{(3)}, \bar{q}_1, q_1^{(1)}$; and the bottom layer includes the remaining six variables $\bar{p}_2^{(1)}, \bar{q}_2^{(1)}, q_1^{(3)}, \bar{p}_2^{(2)}, \bar{q}_2^{(2)}, q_2$. Three Rydberg quantum wires operate on the middle and bottom layers: $\mathbf{P}_4(p_2, w^{(1)}, w^{(2)}, \bar{p}_2^{(1)})$ for $\mathbf{e}(p_2, \bar{p}_2^{(1)})$, $\mathbf{P}_4(q_2, w^{(3)}, w^{(4)}, \bar{q}_2^{(2)})$ for $\mathbf{e}(q_2, \bar{q}_2^{(2)})$, and $\mathbf{P}_8(q_2, w^{(5)}, w^{(6)}, \dots, w^{(10)}, \bar{q}_2^{(1)})$ for $\mathbf{e}(q_2, \bar{q}_2^{(1)})$. The total number of atoms in G_{15}^{Exp} is 24, comprising 14 variable atoms ($p_1^{(1)}, p_2, q_1^{(1)}$, etc.) and 10 quantum-wire atoms ($w^{(1)}, w^{(2)}$, etc.). The atom images of G_{15}^{Exp} are presented in Fig. 3(b) and the 3D coordinates of all atoms are detailed in Table I.

Experimental results of G_{15}^{Exp} are shown in Fig. 3(c). The quantum adiabatic evolution of the Hamiltonian $H(G_{15}^{\text{Exp}})$ is performed, following the experimental procedure outlined in Sec. II. A total of 12 575 experimental events were recorded. We applied the single-vertex error mitigation protocol from Ref. [34] and the Rydberg quantum-wire compilation method of antiferromagnetic chain states from Ref. [26] to obtain 11 274 usable events. The resulting probability distribution is depicted in Fig. 3(d) for all microstates in the basis $|p_1^{(1)}, p_1^{(2)}, p_1^{(3)}, p_2, q_1^{(1)}, q_1^{(2)}, q_1^{(3)}, q_2; \bar{p}_1, \bar{p}_2^{(1)}, \bar{p}_2^{(2)}, \bar{q}_1, \bar{q}_2^{(1)}, \bar{q}_2^{(2)}\rangle$ covering all variable and negation atoms of G_{15}^{Exp} . In Fig. 3(d), the experimental probability distribution $P(p, q)$ is presented

in the $((p_2 p_1 p_0)_2; (q_2 q_1 q_0)_2)$ basis. The standard variable assignment method for duplicate variables [43] was used, wherein a variable x is binary one if any duplicate $x^{(i)}$ is one, and all of its negations $\bar{x}^{(j)}$ s are zero at the same time. Conversely, it is binary zero if all duplicates $x^{(i)}$ are zero, and any variable duplicate $\bar{x}^{(j)}$ is one. If neither condition is met, it is marked as “undecidable.” As a result, the Rydberg-atom experiment involving G_{15}^{Exp} identifies the integer factors of $p \times q = 15$ to be $(p, q) = (3, 5)$ and $(5, 3)$, with probabilities of 13.5(5)% and 16.0(6)%, respectively.

B. Solving $p \times q = 35$

Let us examine another example: $p \times q = 35$. The procedure is similar to the previous $p \times q = 15$ example. The SAT formula Ψ_{35} is derived as follows:

$$\Psi_{35} = p_0 q_0 (p_1 + p_2)(p_1 + q_1)(p_1 + q_2)(\bar{p}_1 + \bar{q}_1) \times (q_1 + q_2 + \bar{p}_1)(p_2 + q_1 + \bar{p}_1 + \bar{q}_2) = 1. \quad (16)$$

It can be reformulated for 3-SAT implementation as

$$\Psi_{35} = p_0 q_0 (p_1 + p_2)(p_1 + q_1)(p_1 + q_2)(\bar{p}_1 + \bar{q}_1) \times (q_1 + q_2 + \bar{p}_1)(p_2 + q_1 + s) \cdot (\bar{p}_1 + \bar{q}_2 + \bar{s}) = 1. \quad (17)$$

TABLE I. Atom positions of G_{15}^{Exp} , G_{35}^{Exp} .

Graphs	Atom positions (x, y, z) or (x, y) (μm)						
G_{15}^{Exp}	$p_1^{(1)}$:	(0.0,6.43,6.43)	$p_1^{(2)}$:	(0.0, -6.43, 6.43)	$p_1^{(3)}$:	(-9.09, 0.0, 0.0)	
	p_2 :	(-1.64, 12.67, 0.0)	$q_1^{(1)}$:	(18.18,0.0,0.0)	$q_1^{(2)}$:	(9.09, -6.43, 6.43)	
	$q_1^{(3)}$:	(9.09, 6.43, -6.43)	q_2 :	(24.61, 0.0, -6.43)	\bar{p}_1 :	(0.0,0.0,0.0)	
	$\bar{p}_2^{(1)}$:	(-13.64, 4.55, -6.43)	$\bar{p}_2^{(2)}$:	(4.55, 14.3, -6.43)	\bar{q}_1 :	(9.09,0.0,0.0)	
	$\bar{q}_2^{(1)}$:	(-13.64, -4.55, -6.43)	$\bar{q}_2^{(2)}$:	(13.64, 14.3, -6.43)	$w^{(1)}$:	(-10.0, 16.31, 0.0)	
	$w^{(2)}$:	(-15.45, 12.73, -6.43)	$w^{(3)}$:	(27.34, 8.67, -6.43)	$w^{(4)}$:	(22.18, 15.85, -6.43)	
	$w^{(5)}$:	(29.61, -7.0, -6.43)	$w^{(6)}$:	(22.73, -13.64, -6.43)	$w^{(7)}$:	(13.64, -13.64, -6.43)	
	$w^{(8)}$:	(4.55, -13.64, -6.43)	$w^{(9)}$:	(-4.55, -13.64, -6.43)	$w^{(10)}$:	(-13.64, -13.64, -6.43)	
	G_{35}^{Exp}	$p_1^{(1)}$:	(35.36,32.14)	$p_1^{(2)}$:	(36.43,43.21)	$p_1^{(3)}$:	(78.21,41.43)
		$p_2^{(1)}$:	(29.29,27.14)	$p_2^{(2)}$:	(62.14,29.29)	$q_1^{(1)}$:	(62.14,48.21)
$q_1^{(2)}$:		(60.36,36.79)	$q_2^{(1)}$:	(42.50,48.21)	$q_2^{(2)}$:	(53.93,47.14)	
$\bar{p}_1^{(1)}$:		(42.14,37.5)	$\bar{p}_1^{(2)}$:	(56.43,53.93)	$\bar{p}_1^{(3)}$:	(73.21,47.14)	
\bar{q}_1 :		(66.79,41.79)	\bar{q}_2 :	(47.86,42.14)	$q_1^{(3)}$:	(71.79,36.43)	
s :		(55.36,33.93)	\bar{s} :	(48.93,34.29)	$w^{(1)}$:	(84.29,47.86)	
$w^{(2)}$:		(80.00,55.00)	$w^{(3)}$:	(73.57,61.07)	$w^{(4)}$:	(64.29,59.29)	
$w^{(5)}$:		(31.43,50.36)	$w^{(6)}$:	(34.64,57.50)	$w^{(7)}$:	(42.50,61.43)	
$w^{(8)}$:		(50.36,61.07)					

This involves replacing the last clause ($p_2 + q_1 + \bar{p}_1 + \bar{q}_2$) in Eq. (16), which has four variables, with ($p_2 + q_1 + s$) ($\bar{p}_1 + \bar{q}_2 + \bar{s}$) by introducing a dummy variable s . The corresponding Rydberg-atom graph G_{35} is given by

$$\begin{aligned}
 G_{35} = & \mathbf{K}_2(p_1^{(1)}, p_2^{(1)}) \cup \mathbf{K}_2(p_1^{(2)}, q_1^{(1)}) \cup \mathbf{K}_2(p_1^{(3)}, q_2^{(1)}) \\
 & \cup \mathbf{K}_2(\bar{p}_1^{(1)}, \bar{q}_1) \cup \mathbf{K}_3(q_1^{(2)}, q_2^{(2)}, \bar{p}_1^{(2)}) \\
 & \cup \mathbf{K}_3(p_2^{(2)}, q_1^{(3)}, s) \cup \mathbf{K}_3(\bar{p}_1^{(3)}, \bar{q}_2, \bar{s}) \\
 & + \sum_{i,j=1}^3 \mathbf{e}(p_1^{(i)}, \bar{p}_1^{(j)}) + \sum_{i=1}^3 \mathbf{e}(q_1^{(i)}, \bar{q}_1) + \sum_{i=1}^2 \mathbf{e}(q_2^{(i)}, \bar{q}_2) \\
 & + \mathbf{e}(s, \bar{s}), \tag{18}
 \end{aligned}$$

as depicted in Fig. 4(a).

Implementing G_{35} directly in an experiment is challenging, even with Rydberg quantum wires. Hence, we explore a 2D version of the experimental graph, denoted as G_{35}^{Exp} , expressed by the following:

$$\begin{aligned}
 G_{35}^{\text{Exp}} = & \mathbf{K}_2(p_1^{(1)}, p_2^{(1)}) \cup \mathbf{K}_2(p_1^{(2)}, q_1^{(1)}) \cup \mathbf{K}_2(p_1^{(3)}, q_2^{(1)}) \\
 & \cup \mathbf{K}_2(\bar{p}_1^{(1)}, \bar{q}_1) \cup \mathbf{K}_3(q_1^{(2)}, q_2^{(2)}, \bar{p}_1^{(2)}) \\
 & \cup \mathbf{K}_3(p_2^{(2)}, q_1^{(3)}, s) \cup \mathbf{K}_3(\bar{p}_1^{(3)}, \bar{q}_2, \bar{s}) \\
 & \cup \mathbf{P}_6(p_2^{(2)}, w^{(1)}, w^{(2)}, w^{(3)}, w^{(4)}, \bar{p}_1^{(2)}) \\
 & \cup \mathbf{P}_6(p_1^{(3)}, w^{(5)}, w^{(6)}, w^{(7)}, w^{(8)}, \bar{p}_1^{(2)}) \\
 & + \mathbf{e}(p_1^{(1)}, \bar{p}_1^{(3)}) + \mathbf{e}(p_1^{(2)}, \bar{p}_1^{(1)}) + \mathbf{e}(p_1^{(3)}, \bar{p}_1^{(3)}) \\
 & + \sum_{i=1}^3 \mathbf{e}(q_1^{(i)}, \bar{q}_1) + \sum_{i=1}^2 \mathbf{e}(q_2^{(i)}, \bar{q}_2) \\
 & + \mathbf{e}(s, \bar{s}), \tag{19}
 \end{aligned}$$

as illustrated in Fig. 4(b). In this representation, the term $\sum_{i,j=1}^3 \mathbf{e}(p_1^{(i)}, \bar{p}_1^{(j)})$ in Eq. (18) is replaced by

$\mathbf{e}(p_1^{(1)}, \bar{p}_1^{(3)}) + \mathbf{e}(p_1^{(2)}, \bar{p}_1^{(1)}) + \mathbf{e}(p_1^{(3)}, \bar{p}_1^{(3)})$. Two Rydberg quantum wires $\mathbf{P}_6(p_1^{(2)}, \dots, \bar{p}_1^{(2)})$ and $\mathbf{P}_6(p_1^{(3)}, \dots, \bar{p}_1^{(2)})$ are introduced for edges $\mathbf{e}(p_1^{(2)}, \bar{p}_1^{(2)})$ and $\mathbf{e}(p_1^{(3)}, \bar{p}_1^{(2)})$, respectively. The remaining four edges, $\mathbf{e}(p_1^{(1)}, \bar{p}_1^{(1)})$, $\mathbf{e}(p_1^{(1)}, \bar{p}_1^{(2)})$, $\mathbf{e}(p_1^{(2)}, \bar{p}_1^{(3)})$, $\mathbf{e}(p_1^{(3)}, \bar{p}_1^{(1)})$, are treated post-selectively. This 2D graph involves a total of 25 atoms, comprising 17 variable atoms and 8 quantum-wire atoms. The atom image is presented in Fig. 4(b) and the 2D coordinates of all atoms are detailed in Table I.

Figure 4(d) showcases the experimental outcomes of G_{35}^{Exp} . The probability distribution is plotted in the basis of all variable and negation atoms of G_{35}^{Exp} . Among the 13 microstates highlighted in blue, there are correct mapping to the solution factors. Conversely, the microstates labeled in black are deemed Ψ_{35} unsatisfiable, and those in gray are considered “undecidable” regarding a definite set of values for variables (p_2, p_1, q_2, q_1, s). Out of 9,383 experimental events, 5,337 usable events were collected after the procedures of the single-vertex error mitigation protocol [34] and the Rydberg quantum-wire compilation method [26] are applied. In contrast to the previous experiment with $p \times q = 15$, where 89.7(5)% of total events are deemed usable, the experiment of $p \times q = 35$ only yields 56.9(5)% usable events. This discrepancy reflects the consequence of post-selective treatment applied to the four edges $\mathbf{e}(p_1^{(1)}, \bar{p}_1^{(1)})$, $\mathbf{e}(p_1^{(1)}, \bar{p}_1^{(2)})$, $\mathbf{e}(p_1^{(2)}, \bar{p}_1^{(3)})$, $\mathbf{e}(p_1^{(3)}, \bar{p}_1^{(1)})$ in G_{35} , but not in G_{35}^{Exp} .

In Fig. 4(e), the probability distribution for solution factors (p, q) is visually presented, employing a color-coding scheme. Probability peaks corresponding to the correct solution factors are highlighted in blue, those for microstates failing to satisfy Ψ_{35} are depicted in black, and the probabilities for “undecidable” microstates are colored in gray. Among the probability peaks showcased in Fig. 4(e), the most prominent peaks associated with solution factors (p, q) are (101,111) and (111,101), with probabilities of 57.6(7)% and 18.8(5)%, respectively, out of 5,003 nongray events. Consequently, the solution to the factor pair in the problem of

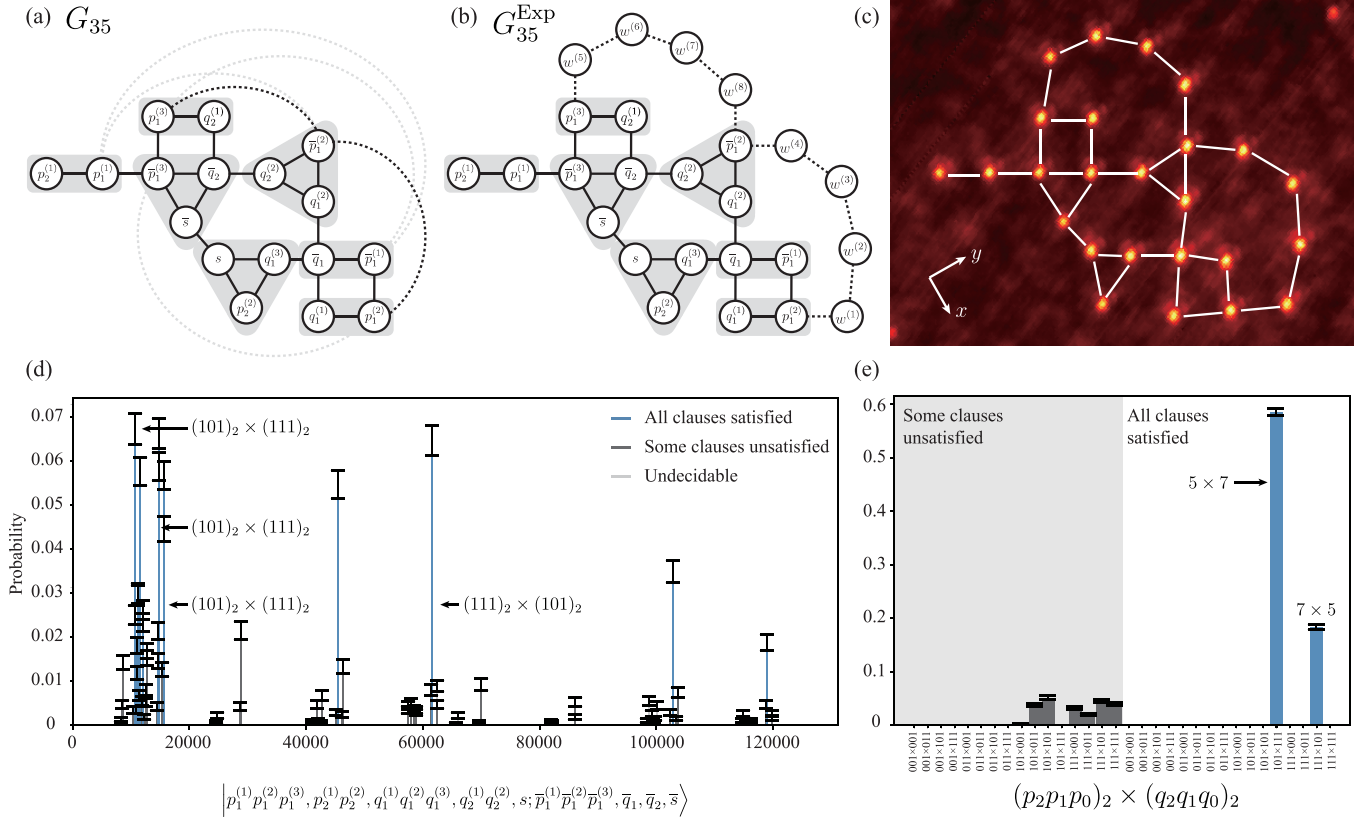


FIG. 4. Implementing the integer factorization of $p \times q = 35$ using Rydberg atoms. (a) Rydberg-atom graph G_{35} . (b) Experimental Rydberg-atom graph G_{35}^{Exp} and (c) the image of the atom configuration. (d) Probability distribution obtained experimentally for all microstates in the basis of variable and negation atoms in G_{35}^{Exp} . The top four most probable microstates in (d) are $|000, 10, 100, 11, 1; 101, 0, 0, 0\rangle$ corresponding to $((p_2 p_1 p_0)_2, (q_2 q_1 q_0)_2) = (101, 111)$; $|000, 11, 100, 11, 0; 100, 0, 0, 1\rangle$ corresponding to $(101, 111)$; $|011, 11, 000, 01, 0; 000, 1, 0, 1\rangle$ corresponding to $(111, 101)$; and $|000, 11, 110, 10, 0; 100, 0, 0, 1\rangle$ corresponding to $(101, 111)$. (e) Result of factorization. The portion of peaks in (d) following the 3-SAT logical constraints is mapped to $(101; 111) = (5, 7)$ and $(111; 101) = (7, 5)$, demonstrating the correct answer to the factoring problem $35 = 5 \times 7$.

factoring $p \times q = 35$ is determined to be $(p, q) = (5, 7)$ or $(7, 5)$ based on the highest probability peaks observed in the experimental results in Fig. 4(e).

V. DISCUSSION

It is worthwhile to discuss scaling issues related to the Rydberg-atom approach to the factorization problem. First, we will provide an estimation of the required number of atoms for encoding the integer factorization problem and then we will consider computational complexities associated with the presented reduction algorithm in the context of a Rydberg-atom experiment.

Atom resource estimation (upper bound). The necessary number of atoms for the integer factorization of $n = p \times q$ in a Rydberg-atom experiment, is estimated as

$$N_{\text{atom}} = 4.88 N_C^{1.8} \approx 7.29 (\log_2 n)^{5.4} \quad (20)$$

in terms of N_C , the number of clauses [33], in the Boolean formula Ψ designed for factoring the given integer n (to be detailed below).

The determination of N_C involves connecting each unit BDD corresponding to $f_{(i', j')}$ in Eq. (11), as illustrated in Fig. 2(b). For simplicity, we omit primes, mapping $i' \mapsto i$ and

$j' \mapsto j$, hereafter. To approximate N_C , let us first compute the number of clauses corresponding to a single generic unit BDD. For example, in an exemplary BDD in Fig. 5(a) for factoring $p \times q = 15$, there are 14 unit BDDs, each of which is represented with an initial running sum v and parameters p_i, q_j , along with auxiliary variables $l_{\text{up}}^{(i, j; v)}, l_{\text{left}}^{(i, j; v)}, l_{\text{right}}^{(i, j; v)} \in \{0, 1\}$. A generic unit BDD shown in Fig. 5(b) corresponds to the assignment of these auxiliary variables for $i = 2, j = 0, v = 7$, extracted from Fig. 5(a). The uppermost initial node of the unit BDD in Fig. 5(b) is assigned $l_{\text{up}}^{(i, j; v)} = 1$ if that node is “passed-through,” and $l_{\text{up}}^{(i, j; v)} = 0$ otherwise. $l_{\text{left}}^{(i, j; v)}$ and $l_{\text{right}}^{(i, j; v)}$ are respectively assigned 1 if the left bottom node and the right bottom node of the unit BDD is “passed-through,” respectively, as given by

$$l_{\text{left}}^{(i, j; v)} = l_{\text{up}}^{(i, j; v)} \cdot \overline{p_i q_j}, \quad (21a)$$

$$l_{\text{right}}^{(i, j; v)} = l_{\text{up}}^{(i, j; v)} \cdot p_i q_j. \quad (21b)$$

These constraints among the auxiliary variables have to be satisfied and can be rewritten in a 3-SAT form as

$$\begin{aligned} \Psi^{(i, j; v)} = & (l_{\text{up}}^{(i, j; v)} + \bar{l}_{\text{left}}^{(i, j; v)}) (\bar{p}_i + \bar{q}_j + \bar{l}_{\text{left}}^{(i, j; v)}) \\ & \times (p_i + \bar{l}_{\text{up}}^{(i, j; v)} + l_{\text{left}}^{(i, j; v)}) (q_j + \bar{l}_{\text{up}}^{(i, j; v)} + l_{\text{left}}^{(i, j; v)}) \end{aligned}$$

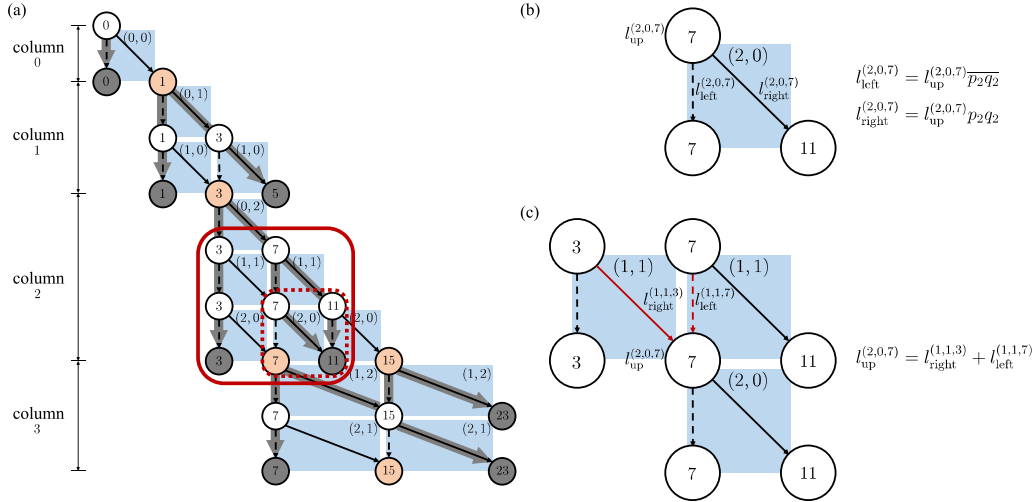


FIG. 5. (a) The binary decision diagram (BDD) designed for factoring $p \times q = 15$. (b) A unit BDD responsible for constructing the 3-SAT formula $\Psi^{(2,0;7)}$. (c) Three unit BDDs collectively constructing the SAT formula $\Phi^{(2,0;7)}$. Refer to the text for a detailed discussion.

$$\begin{aligned} & \times (l_{\text{right}}^{(i,j;v)} + \bar{l}_{\text{up}}^{(i,j;v)} + l_{\text{left}}^{(i,j;v)}) (\bar{l}_{\text{right}}^{(i,j;v)} + l_{\text{up}}^{(i,j;v)}) \\ & \times (\bar{l}_{\text{right}}^{(i,j;v)} + \bar{l}_{\text{left}}^{(i,j;v)}) = 1. \end{aligned} \quad (22)$$

The subsequent step involves establishing logical connections among the “pass-through” variables for various $(i, j; v)$ trios, such as those among $(i, j, v) = (1, 1; 3)$, $(1, 1; 7)$, and $(2, 0; 7)$ in Fig. 5(c). The initial top node of the unit BDD denoted by (i, j) with a running sum v on that node has two incoming edges from the top initial nodes of unit BDDs denoted by (i, j) with running sums $v - 2^{i+j}$ and v . So, a Boolean expression is established among the corresponding “pass-through” variables, $l_{\text{up}}^{(i,j;v)}$, $l_{\text{right}}^{(i-1,j+1;v-2^{i+j})}$, and $l_{\text{left}}^{(i-1,j+1;v)}$, as follows:

$$l_{\text{up}}^{(i,j;v)} = l_{\text{left}}^{(i-1,j+1;v)} + l_{\text{right}}^{(i-1,j+1;v-2^{i+j})}. \quad (23)$$

These constraint for the BDD connections can be rewritten in a 3-SAT form as

$$\begin{aligned} & \Phi_{(i,j;v)}^{(i-1,j+1;v-2^{i+j});(i-1,j+1;v)} \\ & = (\bar{l}_{\text{up}}^{(i,j;v)} + l_{\text{left}}^{(i-1,j+1;v)} + l_{\text{right}}^{(i-1,j+1;v-2^{i+j})}) \\ & \times (l_{\text{up}}^{(i,j;v)} + \bar{l}_{\text{left}}^{(i-1,j+1;v)}) \\ & \times (l_{\text{up}}^{(i,j;v)} + \bar{l}_{\text{right}}^{(i-1,j+1;v-2^{i+j})}) = 1. \end{aligned} \quad (24)$$

Upon collecting all the unit-BDD 3-SAT formulas $\Psi^{(i,j;v)}$ and their connections $\Phi_{(i,j;v)}^{(i-1,j+1;v-2^{i+j});(i-1,j+1;v)}$, and logically multiplying them, we can obtain the total 3-SAT formula Ψ_n for factoring the given integer n . The total number of clauses is then determined by counting the occurrences of the product, each generating $3 + 7 = 10$ clauses in the total 3-SAT formula. Since each unit BDD in Fig. 2(b) consists of three nodes, with two nodes overlapping among neighboring unit BDDs, each unit BDD effectively contributes two nodes to the total BDD. Consequently, the number of unit BDDs in the total BDD is obtained by dividing the total number of nodes in the total BDD by two. The number of nodes in the total BDD

for factoring n , denoted as B_n , is determined by [38]

$$2N_p^3 - 2N_p^2 - 2N_p + 5 \lesssim B_n \lesssim 2N_p^3 - 4N_p + 5, \quad (25)$$

wherein we assume p and q to be $N_p = N_q = \log_2 n/2$ -bit binary integers. Thus, the number of clauses in the total 3-SAT formula is, up to the leading order,

$$N_C = 10 \times (B_n/2) = 10(\log_2 n/2)^3, \quad (26)$$

which results in Eq. (20).

Computational complexity. The classical computational complexity involved in converting the integer factorization problem to a BDD is discussed following the methodology outlined in Ref. [38]. The number of nodes in a total BDD is given by

$$B_n \approx 2(\log_2 n/2)^3, \quad (27)$$

when the BDD consists of $N_0 \equiv (\log_2 n/2)^3$ unit BDD blocks, each with an average 2 nodes, as depicted in Fig. 2(b). The number of time steps required to build each unit BDD of the total BDD for factoring the given integer n and the memory space needed to arrange these unit BDD cells are respectively given by

$$\Delta N_{\text{step}} = N_0, \quad (28)$$

$$\Delta N_{\text{memory}} = N_0. \quad (29)$$

Hence, the construction of a BDD can be accomplished in polynomial time steps and memory space, efficiently using classical computation.

Errors in state preparation, measurement, and imperfect adiabatic evolution. In our present experimental configuration, the errors in state preparation and measurement are quantified as $P(0 \rightarrow 1) = 0.03$ and $P(1 \rightarrow 0) = 0.18$ [26]. In addition, there are also inherent control errors arising from imperfect adiabatic evolution. A heuristic approach introduced in Ref. [34] estimates the successful adiabatic evolution probability p , approximated as $\ln(1-p) \sim HP^{-0.63(13)} \sim e^{-C\sqrt{|G|}}$, where C is a positive constant and $|G|$ is the size of the Rydberg-atom graph. The exponential increase in the

likelihood of unsuccessful adiabatic evolution with $\sqrt{|G|}$ necessitates an enhanced approach beyond the current adiabatic evolution scheme. Nonetheless, recent advancements in error detection, correction, and mitigation [24,44,45] offer prospects for addressing these challenges.

VI. CONCLUSION

These Rydberg-atom experiments have taken on the task of addressing the integer factorization problem, with a particular focus on instances of $p \times q = 6, 15, \text{ and } 35$. The approach involves converting these instances into 3-SAT problems and subsequently mapping them onto Rydberg-atom graphs. These graphs are then subjected to quasiadiabatic quantum experiments, producing superpositions of microstates. These microstates are used to experimentally determine the integer factors (p, q) that constitute $n = p \times q$. The proposed method estimates that the number of required atoms and classical computational resources for obtaining the Rydberg atom graph remain within polynomial orders of $\log_2 n$, suggesting the effectiveness of this encoding scheme. Nonetheless, it is important to note that solving 3-SAT problems on a large scale using Rydberg atoms remains challenging, primarily due to the current limitations of imperfect quantum adiabatic processing hardware.

The experimental data set is archived in Ref. [46] for further analysis.

ACKNOWLEDGMENTS

This research is supported by Samsung Science and Technology Foundation (Grant No. SSTF-BA1301-52). L.V. thanks Sélim Touati for useful discussions.

APPENDIX A: EXPERIMENTAL APPARATUS

The experimental setup closely resembles the one described in Ref. [47]. Optical tweezers are used to trap rubidium atoms (^{87}Rb). These traps are generated using a spatial-light modulator (SLM, ODPDM512 by Meadowlark optics). As outlined in previous work [48], we utilize the Gerchberg-Saxton weighted (GSW) algorithm to generate trap phases for the SLM. Each trap beam is focused by an objective lens with a numerical aperture (NA) of 0.5 (G Plan Apo 50X of Mitutoyo) to a radius of $1.1 \mu\text{m}$. The depth of each trap is approximately 1 mK. To efficiently confine ^{87}Rb atoms in the optical tweezer traps, the atoms are cooled below the trap depth. This cooling process involves initially cooling the atoms in the vacuum chamber using a magneto-optical trap (MOT) before loading them into the traps. Additionally, polarization gradient cooling (PGC) is employed to further cool the atoms to approximately $\sim 30 \mu\text{K}$ inside the optical tweezers. The occupation of atoms is monitored by imaging their fluorescence onto an electron-multiplied-CCD camera (EMCCD, Andor iXon897) while laser-cooling beams are illuminated. An electrically tunable lens (EL-16-40-TC from Optotune) is used to adjust the imaging focal plane to observe the entire three-dimensional atomic array.

Initially, the atoms are randomly loaded into the tweezers due to collisional blockade [49]. Following the imaging of the initial atom loadout in the tweezer traps, vacancies are identified, and the Gerchberg-Saxton algorithm is employed to rearrange atoms from reservoirs to create unity-filling atomic arrays. For excitation to the Rydberg state $|0\rangle = |5S_{1/2}, F = 2, m_F = 2\rangle \rightarrow |1\rangle = |71S_{1/2}, j = 1/2, m_j = 1/2\rangle$, a two-photon transition scheme is utilized with 780-nm (home-built external-cavity diode laser) and 480-nm (TA-SHG Pro from Toptica) lasers via an intermediate level $|5P_{3/2}, F' = 3, m'_F = 3\rangle$ with an intermediate detuning $\Delta_i = (2\pi)660 \text{ MHz}$. Following Rydberg excitation, the population of each atom is measured by illuminating cyclic transition lights, where atoms in $|0\rangle$ exhibit fluorescence while those in $|1\rangle$ do not.

APPENDIX B: ALGORITHM AND HEURISTIC FOR DETERMINING ATOMIC ARRANGEMENT

The algorithm and heuristics are employed to determine the spatial arrangement of atoms corresponding to a given SAT formula Ψ . Given Ψ , we generate a corresponding theoretical Rydberg-atom graph G that initially lacks designated node coordinates.

We first assume that G is planar and has a node degree of at most 4. Any deviations from these will be addressed below. Under this assumption, G can be orthogonally drawn on a 2D plane with a time complexity of $O(|G|^2 \log |G|)$ [50,51]. In this drawing, the appropriate number of atoms for the quantum wire [26] is inserted along the edges, resulting in the realization of G as G_{Exp} , where nodes are assigned real spatial coordinates satisfying the Rydberg blockade interaction criterion outlined in Eq. (7).

If G is not planar, we partition the nodes into different three-dimensional planes. It is guaranteed that any maximum degree 6 graph has drawing on 3 three-dimensional planes [52–54]. We apply this technique of separating nodes into at most 3 three-dimensional planes, as demonstrated in the formation of G_{15}^{Exp} in the text. After that, the method described in the prior paragraph is utilized to form a graph G_{Exp} .

In cases where G contains nodes with a degree exceeding 4, we prune certain edges in G to create another graph G' with a restricted node degree of at most 4. This process ensures that the subgraph H on G , consisting of nodes representing any variable and its negation (e.g., $p_1^{(i)}, \bar{p}_1^{(j)}$ in G_{35} as detailed in the text), remains a connected graph. The resulting graph is then assigned real spatial node coordinates, following the procedure outlined in the previous paragraph, to form G_{Exp} .

APPENDIX C: THE BOOLEAN EXPRESSION FOR $p \times q = 15$

The binary decision diagram (BDD) in Fig. 5(a) is used to derive the SAT formula, Ψ_{15} in Eq. 14. The overall SAT formula for the integer factorization problem is expressed as

$$\Psi_{15} = \Psi_{15,0} \Psi_{15,1} \Psi_{15,2} \Psi_{15,3}, \quad (C1)$$

where $\Psi_{15,0}, \Psi_{15,1}, \Psi_{15,2}$, and $\Psi_{15,3}$ correspond to columns 0, 1, 2, and 3 of the BDD, representing bitwise relations for $p = (p_2 p_1 p_0)_2 \times (q_2 q_1 q_0)_2 = (1111)_2$, respectively. In Fig. 5(a),

the orange-colored circles indicate nodes that need to be “passed-through” for successful factorization of n , while the gray-colored filled circles are not to be “passed-through.”

The unsuccessful path in column 0 corresponds to $\overline{p_0q_0} = 1$. Consequently, the Boolean subformula for column 0 is

$\neg\Psi_{15,0} = \overline{p_0q_0}$ resulting in the Boolean subformula for column 0 in conjunctive normal form:

$$\Psi_{15,0} = p_0q_0. \tag{C2}$$

Similarly, for columns 1 and 2, $\Psi_{15,1}$ and $\Psi_{15,2}$ are obtained by aggregating failed paths in the respective columns:

$$\begin{aligned} \Psi_{15,1} &= \neg(\overline{p_0q_1} \cdot \overline{p_1q_0} + p_0q_1 \cdot p_1q_0) \\ &= (p_0 + p_1)(p_0 + q_0)(q_1 + p_1)(q_1 + q_0)(\overline{p_0} + \overline{q_1} + \overline{p_1} + \overline{q_0}), \end{aligned} \tag{C3}$$

$$\begin{aligned} \Psi_{15,2} &= \neg(\overline{p_0q_2} \cdot \overline{p_1q_1} \cdot \overline{p_2q_0} + \overline{p_0q_2} \cdot p_1q_1 \cdot p_2q_0 + p_0q_2 \cdot \overline{p_1q_1} \cdot p_2q_0 + p_0q_2 \cdot p_1q_1 \cdot \overline{p_2q_0}) \\ &= (p_0q_2 + p_1q_1 + p_2q_0)(p_0q_2 + \overline{p_1q_1} + \overline{p_2q_0})(\overline{p_0q_2} + p_1q_1 + \overline{p_2q_0})(\overline{p_0q_2} + \overline{p_1q_1} + p_2q_0). \end{aligned} \tag{C4}$$

For column 3, paths starting at either the orange-colored “7” node or “15” node on the same horizontal position in Fig. 5(a) are considered. Failed paths $\overline{p_1q_2} \cdot \overline{p_2q_1} = 1$, $p_1q_2 \cdot p_2q_1 = 1$ starting at the orange-colored “7” node, and failed paths $p_1q_2 = 1$, $\overline{p_1q_2} \cdot p_2q_1 = 1$ starting at the “15” node in column 3 are identified. To distinguish between these two distinct failed paths, we introduce auxiliary variables $l_A, l_B \in \{0, 1\}$, with values set to 1 only if the “7” (“15”) node is “passed-through.” The Boolean subformula corresponding to column 3 is then expressed as

$$\begin{aligned} \Psi_{15,3} &= \{l_A \rightarrow \neg(\overline{p_1q_2} \cdot \overline{p_2q_1} + p_1q_2 \cdot p_2q_1)\} \{l_B \rightarrow \neg(p_1q_2 + \overline{p_1q_2} \cdot p_2q_1)\} \\ &= \{l_A \rightarrow (p_1 + p_2)(p_1 + q_1)(q_2 + p_2)(q_2 + q_1)(\overline{p_1} + \overline{q_2} + \overline{p_2} + \overline{q_1})\} \\ &\quad \times \{l_B \rightarrow (\overline{p_1} + \overline{q_2})(p_1 + \overline{p_2} + \overline{q_1})(q_2 + \overline{p_2} + \overline{q_1})\} \\ &= \{\overline{l_A} + (p_1 + p_2)(p_1 + q_1)(q_2 + p_2)(q_2 + q_1)(\overline{p_1} + \overline{q_2} + \overline{p_2} + \overline{q_1})\} \cdot \{\overline{l_B} + (\overline{p_1} + \overline{q_2}) \\ &\quad \times (p_1 + \overline{p_2} + \overline{q_1})(q_2 + \overline{p_2} + \overline{q_1})\}, \end{aligned} \tag{C5}$$

where l_A is expressed in terms of the sum of nonfailed paths in column 2: $\overline{p_0q_2} \cdot p_1q_1 \cdot p_2q_0 = 1$, $\overline{p_0q_2} \cdot p_1q_1 \cdot \overline{p_2q_0} = 1$, and $p_0q_2 \cdot \overline{p_1q_1} \cdot \overline{p_2q_0} = 1$, which lead to the orange-colored “7” node

$$l_A = \overline{p_0q_2} \cdot p_1q_1 \cdot p_2q_0 + \overline{p_0q_2} \cdot p_1q_1 \cdot \overline{p_2q_0} + p_0q_2 \cdot \overline{p_1q_1} \cdot \overline{p_2q_0}, \tag{C6}$$

and l_B is expressed in terms of the nonfailed path $p_0q_2 \cdot p_1q_1 \cdot p_2q_0 = 1$ in column 2, which leads to the “15” node

$$l_B = p_0q_2 \cdot p_1q_1 \cdot p_2q_0. \tag{C7}$$

Substituting l_A, l_B into $\Psi_{15,3}$ yields a Boolean equation in terms only of p, q .

Simplifying Ψ_{15} involves utilizing the fact that $\Psi_{15,0} = p_0q_0 = 1$, as single variable clauses p_0 and q_0 trivially result in values of p_0 and q_0 as 1. Substituting $p_0 = q_0 = 1$, the expressions for $\Psi_{15,1}, \Psi_{15,2}, l_A$, and l_B become

$$\Psi_{15,1} = (p_1 + q_1)(\overline{p_1} + \overline{q_1}), \tag{C8}$$

$$\begin{aligned} \Psi_{15,2} &= (q_2 + p_1q_1 + p_2)(q_2 + \overline{p_1} + \overline{q_1} + \overline{p_2})(\overline{q_2} + p_1q_1 + \overline{p_2})(\overline{q_2} + \overline{p_1} + \overline{q_1} + p_2) \\ &= (q_2 + p_1 + p_2)(q_2 + q_1 + p_2)(q_2 + \overline{p_1} + \overline{q_1} + \overline{p_2})(\overline{q_2} + p_1 + \overline{p_2})(\overline{q_2} + q_1 + \overline{p_2})(\overline{q_2} + \overline{p_1} + \overline{q_1} + p_2) \\ l_A &= \overline{q_2} \cdot p_1q_1 \cdot p_2 + \overline{q_2} \cdot p_1q_1 \cdot \overline{p_2} + q_2 \cdot \overline{p_1q_1} \cdot \overline{p_2} = \overline{q_2}p_1q_1p_2 + \overline{q_2}p_1q_1\overline{p_2} + q_2\overline{p_1}\overline{p_2} + q_2\overline{q_1}\overline{p_2}, \end{aligned} \tag{C9}$$

$$l_B = q_2p_1q_1p_2. \tag{C10}$$

Substituting l_A and l_B into $\Psi_{15,3}$ yields

$$\begin{aligned} \Psi_{15,3} &= \{(q_2 + p_1 + \overline{p_2})(q_2 + q_1 + \overline{p_2})(q_2 + \overline{p_1} + \overline{q_1} + p_2)(\overline{q_2} + p_1 + p_2)(\overline{q_2} + q_1 + p_2) + (p_1 + p_2)(p_1 + q_1) \\ &\quad \times (q_2 + p_2)(q_2 + q_1)(\overline{p_1} + \overline{q_2} + \overline{p_2} + \overline{q_1})\} \{(\overline{q_2} + \overline{p_1} + \overline{q_1} + \overline{p_2}) + (\overline{p_1} + \overline{q_2})(p_1 + \overline{p_2} + \overline{q_1}) \\ &\quad \times (q_2 + \overline{p_2} + \overline{q_1})\} \\ &= (\overline{q_2} + p_1 + p_2)(q_2 + q_1 + \overline{p_2})(\overline{q_2} + \overline{p_1} + \overline{q_1} + \overline{p_2}). \end{aligned} \tag{C11}$$

Multiplying every subformula for each of the columns 0, 1, 2, and 3 results in the following form:

$$\begin{aligned} \Psi_{15} &= p_0q_0 \times (p_1 + q_1)(\overline{p_1} + \overline{q_1})(q_2 + p_1 + p_2)(q_2 + q_1 + p_2)(q_2 + \overline{p_1} + \overline{q_1} + \overline{p_2}) \\ &\quad \times (\overline{q_2} + p_1 + \overline{p_2})(\overline{q_2} + q_1 + \overline{p_2})(\overline{q_2} + \overline{p_1} + \overline{q_1} + p_2)(\overline{q_2} + p_1 + p_2)(q_2 + q_1 + \overline{p_2}) \cdot (\overline{q_2} + \overline{p_1} + \overline{q_1} + \overline{p_2}). \end{aligned} \tag{C12}$$

After simplification using Boolean identities $A(A + B) = A$ and $(A + B)(A + \bar{B}) = A$, the SAT formula corresponding to the problem of factoring $p \times q = 15$ is obtained as

$$\Psi_{15} = (p_1 + p_2)(q_1 + q_2)(\bar{p}_1 + \bar{q}_1)(p_1 + q_1)(p_1 + \bar{p}_2 + \bar{q}_2)(q_1 + \bar{q}_2 + \bar{p}_2)p_0q_0. \quad (\text{C13})$$

-
- [1] R. L. Rivest, A. Shamir, and L. Adleman, A method for obtaining digital signatures and public-key cryptosystems, *Commun. ACM* **21**, 120 (1978).
- [2] P. W. Shor, Algorithms for quantum computation: discrete logarithms and factoring, in *Proceedings of the 35th Annual Symposium on Foundations of Computer Science* (1994), pp. 124.
- [3] D. Beckman, A. N. Chari, S. Devabhaktuni, and J. Preskill, Efficient networks for quantum factoring, *Phys. Rev. A* **54**, 1034 (1996).
- [4] L. M. K. Vandersypen, M. Steffen, G. Breyta, C. S. Yannoni, M. H. Sherwood, and I. L. Chuang, Experimental realization of Shor's quantum factoring algorithm using nuclear magnetic resonance, *Nature (London)* **414**, 883 (2001).
- [5] T. Monz, D. Nigg, E. A. Martinez, M. F. Brandl, P. Schindler, R. Rines, S. X. Wang, I. L. Chuang, and R. Blatt, Realization of a scalable Shor algorithm, *Science* **351**, 1068 (2016).
- [6] U. Skosana and M. Tame, Demonstration of Shor's factoring algorithm for $N = 21$ on IBM quantum processors, *Sci. Rep.* **11**, 16599 (2021).
- [7] B. Yan, Z. Tan, S. Wei, H. Jiang, W. Wang, H. Wang, L. Luo, Q. Duan, Y. Liu, W. Shi, Y. Fei, X. Meng, Y. Han, Z. Shan, J. Chen, X. Zhu, C. Zhang, F. Jin, H. Li, C. Song, Z. Wang, Z. Ma, H. Wang, and G. L. Long, Factoring integers with sublinear resources on a superconducting quantum processor, [arXiv:2212.12372](https://arxiv.org/abs/2212.12372).
- [8] C.-Y. Lu, D. E. Browne, T. Yang, and J.-W. Pan, Demonstration of a compiled version of Shor's quantum factoring algorithm using photonic qubits, *Phys. Rev. Lett.* **99**, 250504 (2007).
- [9] B. P. Lanyon, T. J. Weinhold, N. K. Langford, M. Barbieri, D. F. V. James, A. Gilchrist, and A. G. White, Experimental demonstration of a compiled version of Shor's algorithm with quantum entanglement, *Phys. Rev. Lett.* **99**, 250505 (2007).
- [10] T. Albash and D. A. Lidar, Adiabatic quantum computation, *Rev. Mod. Phys.* **90**, 015002 (2018).
- [11] X. Peng, Z. Liao, N. Xu, G. Qin, X. Zhou, D. Suter, and J. Du, Quantum adiabatic algorithm for factorization and its experimental implementation, *Phys. Rev. Lett.* **101**, 220405 (2008).
- [12] N. Xu, J. Zhu, D. Lu, X. Zhou, X. Peng, and J. Du, Quantum factorization of 143 on a dipolar-coupling nuclear magnetic resonance system, *Phys. Rev. Lett.* **108**, 130501 (2012).
- [13] A. Saxena, A. Shukla, and A. Pathak, A hybrid scheme for prime factorization and its experimental implementation using IBM quantum processor, *Quantum Inf. Process.* **20**, 112 (2021).
- [14] S. Jiang, K. A. Britt, A. J. McCaskey, T. S. Humble, and S. Kais, Quantum annealing for prime factorization, *Sci. Rep.* **8**, 17667 (2018).
- [15] M. Saffman, T. G. Walker, and K. Mølmer, Quantum information with Rydberg atoms, *Rev. Mod. Phys.* **82**, 2313 (2010).
- [16] X. Wu, X. Liang, Y. Tian, F. Yang, C. Chen, Y.-C. Liu, M. Khoon, and L. You, A concise review of Rydberg atom based quantum computation and quantum simulation, *Chin. Phys. B* **30**, 020305 (2021).
- [17] M. Morgado and S. Whitlock, Quantum simulation and computing with Rydberg-interacting qubits featured, *AVS Quantum Sci.* **3**, 023501 (2021).
- [18] M. Kim, J. Ahn, Y. Song, J. Moon, and H. Jeong, Quantum computing with Rydberg atom graphs, *J. Korean Phys. Soc.* **82**, 827 (2023).
- [19] S. Ebadi, T. T. Wang, H. Levine, A. Keesling, G. Semeghini, A. Omran, D. Bluvstein, R. Samajdar, H. Pichler, W. W. Ho, S. Choi, S. Sachdev, M. Greiner, V. Vuletic, and M. D. Lukin, Quantum phases of matter on a 256-atom programmable quantum simulator, *Nature (London)* **595**, 227 (2021).
- [20] P. Scholl, M. Schuler, H. J. Williams, A. A. Eberharter, D. Barredo, K.-N. Schymik, V. Lienhard, L.-P. Henry, T. C. Lang, T. Lahaye, A. M. Läuchli, and A. Browaeys, Quantum simulation of 2D antiferromagnets with hundreds of Rydberg atoms, *Nature (London)* **595**, 233 (2021).
- [21] G. Semeghini, H. Levine, A. Keesling, S. Ebadi, T. T. Wang, D. Bluvstein, R. Verresen, H. Pichler, M. Kalinowski, R. Samajdar, A. Omran, S. Sachdev, A. Vishwanath, M. Greiner, V. Vuletic, and M. D. Lukin, Probing topological spin liquids on a programmable quantum simulator, *Science* **374**, 1242 (2021).
- [22] D. Bluvstein, H. Levine, G. Semeghini, T. T. Wang, S. Ebadi, M. Kalinowski, A. Keesling, N. Maskara, H. Pichler, M. Greiner, V. Vuletic, and M. D. Lukin, A quantum processor based on coherent transport of entangled atom arrays, *Nature (London)* **604**, 451 (2022).
- [23] C. Chen, G. Bornet, M. Bintz, G. Emperauger, L. Leclerc, V. S. Liu, P. Scholl, D. Barredo, J. Hauschild, S. Chatterjee, M. Schuler, A. M. Läuchli, M. P. Zaletel, T. Lahaye, N. Y. Yao, and A. Browaeys, Continuous Symmetry Breaking in a Two-dimensional Rydberg Array, *Nature (London)* **616**, 691 (2023).
- [24] D. Bluvstein, S. J. Evered, A. A. Geim, S. H. Li, H. Zhou, T. Manovitz, S. Ebadi, M. Cain, M. Kalinowski, D. Hangleiter, J. P. Bonilla Ataides, N. Maskara, I. Cong, X. Gao, P. Sales Rodriguez, T. Karolyshyn, G. Semeghini, M. J. Gullans, M. Greiner, V. Vuletic *et al.*, Logical quantum processor based on reconfigurable atom arrays, *Nature (London)* **626**, 58 (2023).
- [25] T. M. Graham, Y. Song, J. Scott, C. Poole, L. Phuttitarn, K. Jooya, P. Eichler, X. Jiang, A. Marra, B. Grinkemeyer, M. Kwon, M. Ebert, J. Cherek, M. T. Lichtman, M. Gillette, J. Gilbert, D. Bowman, T. Ballance, C. Campbell, E. D. Dahl *et al.*, Multi-qubit entanglement and algorithms on a neutral-atom quantum computer, *Nature (London)* **604**, 457 (2022).

- [26] M. Kim, K. Kim, J. Hwang, E.-G. Moon, and J. Ahn, Rydberg quantum wires for maximum independent set problems, *Nat. Phys.* **18**, 755 (2022).
- [27] X. Qiu, P. Zoller, and X. Li, Programmable quantum annealing architectures with Ising quantum wires, *PRX Quantum* **1**, 020311 (2020).
- [28] M. T. Nguyen, J. G. Liu, J. Wurtz, M. D. Lukin, S. T. Wang, and H. Pichler, Quantum optimization with arbitrary connectivity using Rydberg atom arrays, *PRX Quantum* **4**, 010316 (2023).
- [29] S. Stastny, H. P. Buchler, and N. Lang, Functional completeness of planar Rydberg blockade structures, *Phys. Rev. B* **108**, 085138 (2023).
- [30] H. Labuhn, S. Ravets, D. Barredo, L. Beguin, F. Nogrette, T. Lahaye, and A. Browaeys, Single-atom addressing in microtraps for quantum-state engineering using Rydberg atoms, *Phys. Rev. A* **90**, 023415 (2014).
- [31] A. Omran, H. Levine, A. Keesling, G. Semeghini, T. T. Wang, S. Ebadi, H. Bernien, A. S. Zibrov, H. Pichler, S. Choi, J. Cui, M. Rossignolo, P. Rembold, S. Montangero, T. Calarco, M. Endres, M. Greiner, V. Vuletic, and M. D. Lukin, Generation and manipulation of Schrödinger cat states in Rydberg atom arrays, *Science* **365**, 570 (2019).
- [32] A. Byun, M. Kim, and J. Ahn, Finding the maximum independent sets of platonic graphs using Rydberg atoms, *PRX Quantum* **3**, 030305 (2022).
- [33] S. Jeong, M. Kim, M. Hhan, J. Y. Park, and J. Ahn, Quantum programming of the satisfiability problem with Rydberg atom graphs, *Phys. Rev. Res.* **5**, 043037 (2023).
- [34] S. Ebadi, A. Keesling, M. Cain, T. T. Wang, H. Levine, D. Bluvstein, G. Semeghini, A. Omran, J.-G. Liu, R. Samajdar, X.-Z. Luo, B. Nash, X. Gao, B. Barak, E. Farhi, S. Sachdev, N. Gemelke, L. Zhou, S. Choi, H. Pichler *et al.*, Quantum optimization of maximum independent set using Rydberg atom arrays, *Science* **376**, 1209 (2022).
- [35] E. Urban, T. A. Johnson, T. Henage, L. Isenhower, D. D. Yavuz, T. G. Walker, and M. Saffman, Observation of Rydberg blockade between two atoms, *Nat. Phys.* **5**, 110 (2009).
- [36] A. Gaëtan, Y. Miroshnychenko, T. Wilk, A. Chotia, M. Viteau, D. Comparat, P. Pillet, A. Browaeys, and P. Grangier, Observation of collective excitation of two individual atoms in the Rydberg blockade regime, *Nat. Phys.* **5**, 115 (2009).
- [37] H. Pichler, S. T. Wang, L. Zhou, S. Choi, M. D. Lukin, Quantum optimization for maximum independent set using Rydberg atom arrays, [arXiv:1808.10816](https://arxiv.org/abs/1808.10816).
- [38] H. Raddum and S. Varadharajan, Factorization using binary decision diagrams, *Cryptogr. Commun.* **11**, 443 (2019).
- [39] S. Russell and P. Norvig, *Artificial Intelligence: A Modern Approach* (Prentice Hall, Englewood Cliffs, 2003).
- [40] M. Srebrny, Factorization with Sat-classical propositional calculus as a programming environment, <https://www.mimuw.edu.pl/~mati/fsat-20040420.pdf> (2004).
- [41] M. Kim, Y. Song, J. Kim, and J. Ahn, Quantum Ising Hamiltonian programming in trio, quartet, and sextet qubit systems, *PRX Quantum* **1**, 020323 (2020).
- [42] Y. Song, M. Kim, H. Hwang, W. Lee, and J. Ahn, Quantum simulation of Cayley-tree Ising Hamiltonians with three-dimensional Rydberg atoms, *Phys. Rev. Res.* **3**, 013286 (2021).
- [43] S. Dasgupta, C. Papadimitriou, and U. Vazirani, *Algorithms* (McGraw-Hill, New York, 2006).
- [44] P. Scholl, A. L. Shaw, R. B. Tsai, R. Finkelstein, J. Choi, and M. Endres, Erasure conversion in a high-fidelity Rydberg quantum simulator, *Nature (London)* **622**, 273 (2023).
- [45] S. Ma, G. Liu, P. Peng, B. Zhang, S. Jandura, J. Claes, A. P. Burgers, G. Pupillo, S. Puri, and J. D. Thompson, High-fidelity gates and mid-circuit erasure conversion in an atomic qubit, *Nature (London)* **622**, 279 (2023).
- [46] J. Park and J. Ahn, Items, figshare, Dataset, <https://doi.org/10.6084/m9.figshare.24603162.v2> (2023).
- [47] K. Kim, M. Kim, J. Park, A. Byun, and J. Ahn, Quantum computing dataset of maximum independent set problem on king lattice of over hundred Rydberg atoms, *Sci. Data* **11**, 111 (2024).
- [48] H. Kim, M. Kim, W. Lee, and J. Ahn, Gerchberg-Saxton algorithm for fast and efficient atom rearrangement in optical tweezer traps, *Opt. Express* **27**, 2184 (2019).
- [49] N. Schlosser, G. Reymond, and P. Grangier, Collisional blockade in microscopic optical dipole traps, *Phys. Rev. Lett.* **89**, 023005 (2002).
- [50] P. Klose, A Generic Framework for the Topology-Shape-Metrics Based Layout, Cristian-Albrechts-Universität zu Kiel (2012).
- [51] R. Tamassia, On embedding a graph in the grid with the minimum number of bends, *SIAM J. Comput.* **16**, 421 (1987).
- [52] P. Eades, C. Stirk, and S. Whitesides, The techniques of komolgorov and bardzin for three-dimensional orthogonal graph drawings, *Inf. Process. Lett.* **60**, 97 (1996).
- [53] T. Biedl, J. R. Johansen, T. Shermer, and D. R. Wood, Orthogonal drawings with few layers, in *Graph Drawing: 9th International Symposium, GD 01* (Springer, New York, 2002), p. 2.
- [54] C. Dalyac, L. P. Henry, M. Kim, J. Ahn, and L. Henriët, Exploring the impact of graph locality for the resolution of the maximum-independent-set problem with neutral atom devices, *Phys. Rev. A* **108**, 052423 (2023).